Chapter 4

Simplified Power Angle Control of UPQC-DG

4.1 Preamble

UPQC control involves extraction of distorted components of supply voltage and current and injecting the complementary distorted components into distribution system through series and shunt APFs to make these quantities balanced, sinusoidal with unity power factor. For extraction of distorted components various techniques, such as Instantaneous Reactive Power theory (IRP or p-q theory), Synchronous Reference Frame theory (SRF or d-q theory) and Enhanced Phase Locked Loop (EPLL) have been used [1, 2]. Control of UPQC-DG based on p-q theory has been used extensively for integration of solar PV [3–5]. IRP based control is simple and fast, since it doesn't involve any complex computational block such as PLL, but it doesn't perform well in non-ideal grid voltage conditions [1]. SRF (d-q) theory based control, which uses a Phase Locked Loop (PLL) to take care of supply voltage distortions, is proposed for PV based UPQC-DG, but attention is not given to efficient utilization of ratings of series and shunt APFs [6, 7].

VA rating of series APF is under-utilized if it compensates only for transient grid disturbances such as voltage sag and swell. So Power Angle Control (PAC), which aims at effective utilization of VA ratings of series and shunt APF of UPQC has been proposed [8–10]. In PAC, series APF provides part of load reactive power by injecting voltage at angle with source current, unlike conventional control in which series APF injects voltage in phase with source current. Out of phase injection of series voltage introduces a phase angle between load voltage and source voltage, commonly known as power angle. During voltage sag or swell, series APF in PAC approach compensates for sag or swell along with providing part of load reactive

power either by keeping power angle constant or varying it suitably [11].

PAC method of UPQC in works [4, 10, 11] is based on IRP theory (p-q theory), which makes this method sensitive to non-ideal supply voltages. So SRF theory (d-q theory) based PAC method for UPQC has been developed [12], but sag/swell compensation is not considered in control of series APF. SRF based PAC method, which shares load reactive powerlly between series and shunt APF has been developed to achieve equal VA loading of these APFs [13], but method is complex and gives accurate results only with small values of power angle. Apart from this, above-mentioned two PAC methods are not directly applicable to UPQC-DG, since they require to accommodate power generated by DG.

PAC control method is especially significant in case of UPQC-DG as shunt APF of UPQC-DG supplies power generated by DG and reactive power demand of load. PAC approach reduces burden of shunt APF by sharing its reactive power burden with series APF, which has no VA burden in normal conditions of grid voltage. PAC control of UPQC-DG based on p-q theory has been simulated for grid integration of solar PV [14], but method requires balanced and harmonic free supply voltages and detailed modeling of solar PV generation system has not been considered.

In present chapter, a new SRF based PAC approach for solar PV based UPQC-DG has been proposed. Proposed PAC method has following salient features:

- Proposed technique employs a simple less computationally intensive method for power calculation and power angle estimation.
- Proposed technique has fast transient response due to less computation.
- It supports large values of power angle. Upper limit on power angle is decided by rating of series APF.

Apart from this, equivalent circuit model of solar PV is incorporated for a more realistic simulation. Furthermore, Opal-RT based Real Time Digital Simulation (RTDS) is carried out to validate performance of the proposed method. In RTDS, electrical circuit of UPQC-DG is simulated on FPGA with sub-microsecond time step to emulate physical hardware for better validation of proposed controller.

The rest of chapter is organized as follows: Section 4.2 describes configuration of solar PV based UPQC-DG. Section 4.3 gives mathematical analysis of PAC method of UPQC. Section 4.4 covers proposed PAC based control method of UPQC-DG. Section 4.5 presents simulation framework and test case data. Detailed steady state

and dynamic simulation results are presented in section 4.6 and section 4.7 concludes the chapter.

4.2 Configuration of Solar PV based UPQC-DG

In this work, solar PV is selected as DG source due to its renewable and environment friendly nature. PV array is connected at DC link of UPQC-DG via a boost DC-DC converter as shown in Fig. 4.1. This configuration of UPQC-DG is based upon three phase three wire supply system, which is most common in distribution system. This configuration has three major components or Power Electronic Converters: shunt APF, series APF and DC-DC boost Converter. Both series and shunt APFs are IGBT based three phase three leg bridge inverters sharing a common DC link. Single phase series injection transformers are used in each phase to inject voltage produced by series APF. Interfacing inductors are used at the output of each APF.

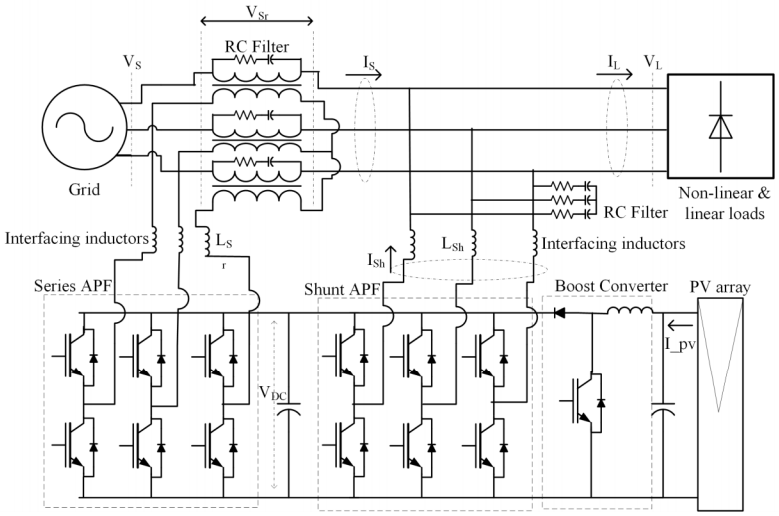

Figure 4.1: Configuration of UPQC-DG with solar PV connected to DC link via a boost converter

High pass RC filters are used at the output of series and shunt APFs to filter out high frequency components in voltage or current, generated by PWM switching of these APFs. RC time constant of these filters is kept small so that high frequency components will pass through them.

UPQC-DG configuration has certain advantages over conventional UPQC. In UPQC-DG shunt APF feeds power available from solar PV to load eliminating additional solar inverter (which is costly). Also filter capacitor at the output of boost converter is not required as there is already a large capacitor connected at DC link of UPQC-DG.

4.3 Analysis of PAC Method

Voltage based phasor diagram of PAC approach for phase a quantities is shown in Fig. 4.2. V_S is nominal supply voltage (rms value equals to k). In normal operation load voltage (V_L) makes an angle δ with source voltage(rms value equals to that of V_S). Series voltage (V_{Sr})injected by series APF is a phasor difference of load voltage and source voltage.

On occurrence of sag, magnitude (rms) of supply voltage is reduced to k'. If power angle δ is held fixed then series voltage (V'_{Sr}) injected during sag will have less magnitude than V_{Sr} injected during normal operation. Reverse is the case when swell occurs on the system. During swell series voltage (V''_{Sr}) has highest magnitude among three cases as shown in Fig. 4.2. Thus if fixed power angle method is used then rating of series APF should be selected based on swell condition. The disadvantage of this technique is that swell occurrence is rare thus series APF rating will be under utilized during sag and normal operation.

In variable PAC method, δ value is changed when sag or swell occurs. Series APF operates at its full rating during normal operation if there is sufficient demand of reactive power from load. On occurrence of sag or swell this power angle is changed in such a way that series APF still operates at its full capacity.

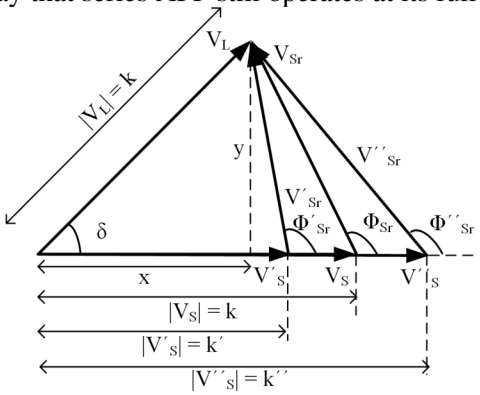

Figure 4.2: Phasor diagram of UPQC under PAC approach

From Fig. 4.2 following equations can be derived under sag condition:

$$x = k cos\delta \tag{4.1}$$

$$y = k sin\delta \tag{4.2}$$

$$|V'_{Sr}| = \sqrt{y^2 + (k' - x)^2} \tag{4.3}$$

$$|V'_{Sr}| = \sqrt{k^2 + k'^2 - 2kk' cos\delta} \tag{4.4}$$

Assuming f_S to be fraction of voltage sag, and f_{Sr} to be ratio of series voltage (V'_{Sr}) to rated source voltage k, further simplifications lead to following expressions:

$$f_S = k'/k \tag{4.5}$$

$$f_{Sr} = |V'_{Sra}|/k \tag{4.6}$$

$$f_{Sr} = \sqrt{1 + {f_S}^2 - 2 f_S cos\delta} \tag{4.7}$$

$$\delta = \cos^{-1}\left[\frac{1 + {f_S}^2 - {f_{Sr}}^2}{2 f_S}\right] \tag{4.8}$$

From equation (8) it can be observed that if series APF is supplying rated voltage ($V_{Sr,max}$) then δ will be at its maximum value at a particular supply voltage:

$$\delta_{max} = \cos^{-1}\left[\frac{1 + {f_S}^2 - {f_{Sr,max}}^2}{2 f_S}\right] \tag{4.9}$$

It is to be noted that δ_{max} is not a fixed value, rather it varies with variation in supply voltage due to presence of f_S in Eq. 4.9. Actual value of δ in case of normal UPQC is calculated from reactive power (Q_{Sr}) supplied by series APF and load active power (P_L) using Eq. 4.10 [10].

$$\delta = \sin^{-1}\left(\frac{Q_{Sr}}{P_L}\right) \tag{4.10}$$

But in case of UPQC-DG since part of load active power is supplied by DG through shunt APF, effective load power as seen by series APF will be difference of two. So power angle in case of solar PV based UPQC-DG may be computed as:

$$\delta = \sin^{-1}\left(\frac{Q_{Sr}}{P_L - P_{PV}}\right) \tag{4.11}$$

Where maximum reactive power handled by series APF under normal supply

voltage conditions may be computed from Eq. 4.12, which can be derived from Eq. 4.11.

$$Q_{Sr,max} = (P_L - P_{PV}) \sin \delta_{max} \tag{4.12}$$

Rest of the reactive power demand of load is to be supplied by shunt APF of UPQC.

4.4 Control of PV based UPQC-DG using PAC Approach

Series APF injects compensating voltages and shunt APF injects compensating currents & also performs task of DC link voltage regulation in UPQC. In UPQC-DG shunt APF has additional task of feeding DG power to load. DC-DC converter gives necessary change in voltage level for connecting DG to DC link and provides duty ratio control to extract maximum power from DG such as solar PV and wind. Details of control of each of these converters are described as follows:

4.4.1 Series APF Control

In PAC approach, series APF injects suitable series voltage to compensate for power quality issues in supply voltage and to supply a part of load reactive power. In order to supply a part of load reactive power series voltage should be injected at a particular angle with supply current, resulting in phase difference between load voltage and supply voltage. For generating reference signals, load voltage phase angle (power angle) with respect to source current/voltage is to be estimated.

Block diagram for estimation of power angle is shown in Fig. 4.3. Instantaneous value of power angle is computed from values of load active power, power generated from PV and load reactive power using Eq. 4.11. Since denominator in Eq. 4.11 can become zero, a limiter is used to avoid such cases. Estimation of instantaneous load power (active and reactive) and PV power is done using already available measurements of UPQC-DG controller. Load active power can be estimated from instantaneous three phase load voltages and currents:

$$P_L = v_{La} i_{La} + v_{Lb} i_{Lb} + v_{Lc} i_{Lc} \tag{4.13}$$

In a balanced three phase system, line to line voltages are at ninety degree with corresponding phase voltages, load reactive power can be computed from line to line load voltages and per phase load currents:

$$Q_L = (v_{Lbc} i_{La} + v_{Lca} i_{Lb} + v_{Lab} i_{Lc})/3 \tag{4.14}$$

Because values of P_L and Q_L are oscillatory especially in case of non-linear loads, low pass filters are used to extract their average values. Power generated by solar PV is computed using output voltage and current (both of which are DC quantities) of PV array:

$$P_{PV} = V_{PV} I_{PV} \tag{4.15}$$

As maximum power angle (δ_{max}) varies with supply voltage, its instantaneous value is calculated using Eq. 4.9. In this equation a limiter is used to avoid denominator becoming zero. Power angle (δ_C, calculated using Eq. 4.11) is compared to δ_{max} and minimum of the two is selected as final δ_F for control of series APF.

Control of Series APF is implemented using Unit Vector Template Generation (UVTG) technique [15]. In this technique no PI controller is required (Fig. 4.3), eliminating the need to tune PI, which saves design effort. A three phase PLL is used to generate *wt* corresponding to fundamental component of phase A. Generated *wt* is then added with δ_F estimated using power angle estimator block, and their sum is utilized to generate three phase balanced unit vectors (time varying sinusoidal signals with unit amplitude) using Eq. 4.16.

$$\begin{bmatrix} U_a \\ U_b \\ U_c \end{bmatrix} = \begin{bmatrix} sin(\omega t + \delta_F) \\ sin(\omega t + \delta_F - 2\pi/3) \\ sin(\omega t + \delta_F + 2\pi/3) \end{bmatrix} \tag{4.16}$$

The desired (reference) amplitude of load voltage is multiplied with these unit vectors to generate reference load voltage signals, which are phase displaced from source voltages by angle δ_F. Sensed load voltage signals and reference load voltage signals are then fed to voltage PWM controller of series APF.

4.4.2 Shunt APF Control

Shunt APF of UPQC-DG injects compensating currents as well as current generated from DG and handles current required for maintaining DC link voltage (Fig. 4.3). For generating reference signals corresponding to compensating currents SRF theory based extraction method is used. In this method first three phase load currents are transformed from abc frame to dq0 frame using Park's transform (Eq. 4.17), *wt* signal required for this transformation is generated using a three phase PLL on source voltages.

$$\begin{bmatrix} I_{Ld} \\ I_{Lq} \\ I_{L0} \end{bmatrix} = \frac{2}{3} \begin{bmatrix} sin\omega t & sin(\omega t - \frac{2\pi}{3}) & sin(\omega t + \frac{2\pi}{3}) \\ cos\omega t & cos(\omega t - \frac{2\pi}{3}) & cos(\omega t + \frac{2\pi}{3}) \\ 1/2 & 1/2 & 1/2 \end{bmatrix} \begin{bmatrix} I_{La} \\ I_{Lb} \\ I_{Lc} \end{bmatrix} \tag{4.17}$$

Park's transform converts fundamental & in phase component of AC quantities into DC quantity which is easily extracted using low pass filters. Ideally, source current supplies this fundamental & in phase component, which serves to build reference source current signals, which are free from power quality issues. Current generated by PV array is subtracted from extracted d-axis component of load current (PV supplies power where as load consumes the power). Current required for maintaining DC link voltage is estimated using a PI controller and added to d-axis load current. The resultant d-axis current is then transformed into three phase balanced sinusoidal reference source currents using inverse Park's transform (Eq. 4.18). Reference and measured source currents are passed through a hysteresis controller to generate switching pulses for shunt APF.

$$\begin{bmatrix} {I_{sa}}^* \\ {I_{sb}}^* \\ {I_{sc}}^* \end{bmatrix} = \begin{bmatrix} sin\omega t & cos\omega t & 1 \\ sin(\omega t - \frac{2\pi}{3}) & cos(\omega t - \frac{2\pi}{3}) & 1 \\ sin(\omega t + \frac{2\pi}{3}) & cos(\omega t + \frac{2\pi}{3}) & 1 \end{bmatrix} \begin{bmatrix} {I_d}^* \\ {I_q}^* \\ {I_0}^* \end{bmatrix} \tag{4.18}$$

4.4.3 DC-DC Converter Control

A boost DC-DC converter is used to interface solar PV to DC link of UPQC-DG. This boost converter has two functions: to step up the voltage generated at PV terminals to DC link voltage, and to extract maximum available power from solar PV using Maximum Power Point Tracking (MPPT) control. There are different MPPT algorithms available for solar PV such as Perturb and Observe (P&O) algorithm and Incremental

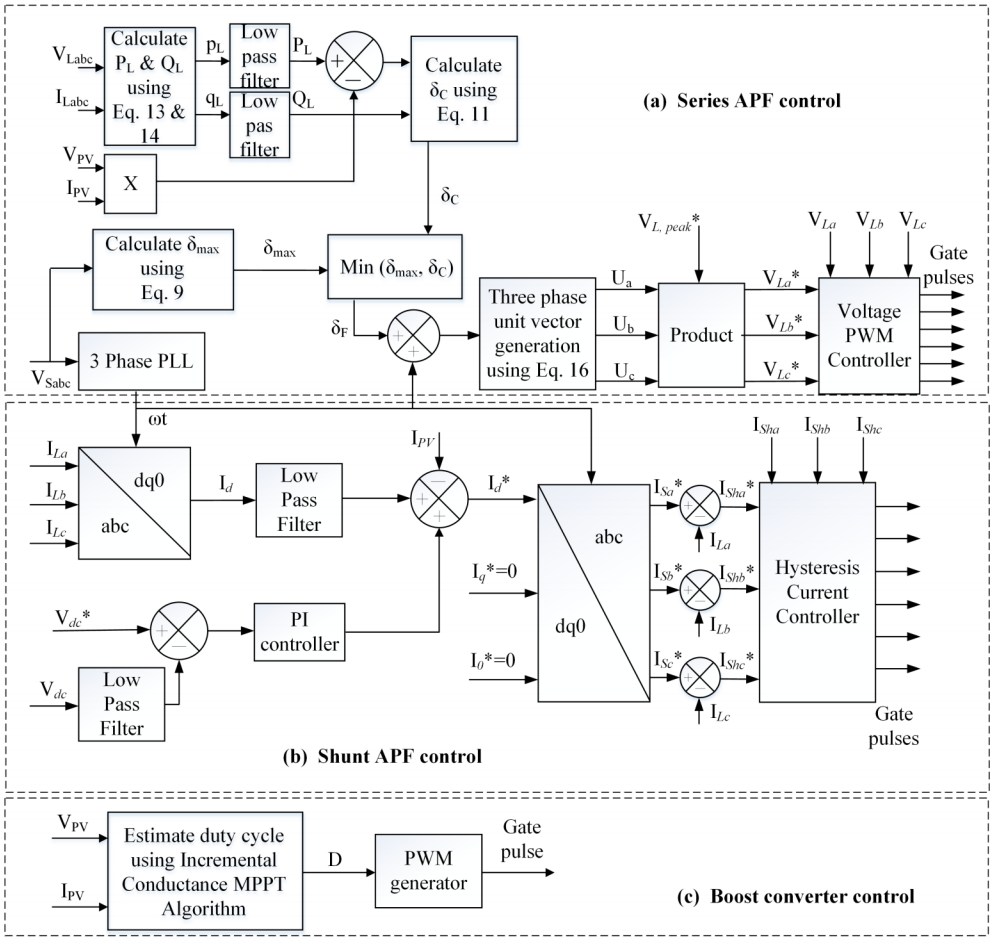

Figure 4.3: Control of UPQC-DG

Conductance (IC) algorithm. MPPT method used in this work for control of boost converter is Incremental Conductance algorithm with integral regulator [16]. From P-V curve of solar PV $dP/dV = 0$, at Maximum Power Point (MPP). This yields:

$$\frac{dI}{dV} = -\frac{I}{V} \tag{4.19}$$

Integral regulator minimizes the error $(dI/dV + I/V)$ and gives required correction in duty cycle in order to track MPP accurately.

4.5 Real Time Simulation Framework and System Data

Simulation of proposed PAC control of UPQC-DG has been carried out in Opal-RT. Details of the simulation and case study system are given in following subsections:

4.5.1 Simulation Framework

Real time simulation has been carried out in Opal-RT simulator OP-4510 (Fig. 4.4). This simulator has two processing units: (1) CPU core (2) FPGA computational engine. In this work FPGA engine of Opal-RT is used for simulating plant (electrical circuit) of UPQC-DG. FPGA being fast, offers sub-microsecond time steps for simulating fast responding power electronic circuits [17]. CPU core is used for simulating proposed control algorithm with time step of 15 microseconds. Control unit of UPQC-DG, implemented on CPU core, recieves measurements from electrical circuit, which runs on FPGA. In response to measurements, control unit provides control signals or switching pulses to electrical cuircuit part. Simulation results are obtained on analog outputs of simulator. The recorded simulation results are sent to host PC after completion of simulation.

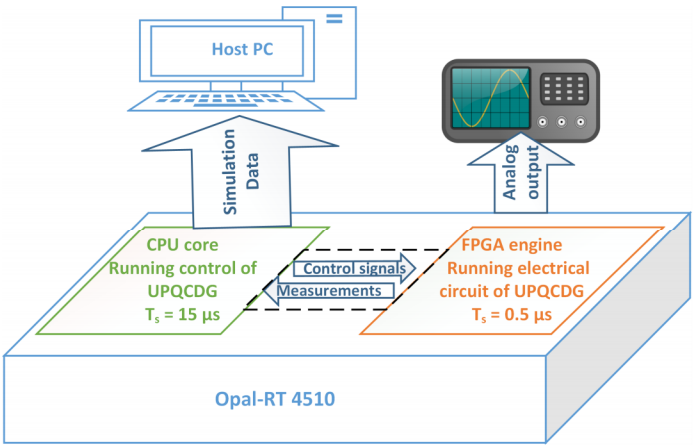

Figure 4.4: Real time simulation setup using Opal-RT

4.5.2 Case Study System

Parameters of UPQC-DG system shown in Fig. 4.1 are calculated using procedure elaborated in [6] and the selected values of these parameters are shown in Table 4.1,. Three phase grid supply is selected as 415 V, 50 Hz with source resistance R_S and

Table 4.1: Parameters of UPQC-DG

3 Phase supply	415 V, 50 Hz, R_S = .05 Ω, L_S = 0.25 mH
DC link	V_{DC} = 700 V, C_{DC} = 5500 μF
Shunt APF	42 kVA, L_C = 1.5 mH
Series APF	29 kVA, n_T = 1, S_T = 2.5 kVA
Boost Converter	V_I = 500-550 V, V_O = 700 V, L_b = 5 mH
Load-1	thyristor bridge rectifier (R = 26 Ω)
Load-2	3-phase R-L load (20 kW, 0.707 p.f. lagging)
Load-3	3-phase R-L load (10 kW, 0.707 p.f. lagging)

inductance L_S. Load-1, a non-linear load, is made of a three phase diode bridge rectifier supplying a DC load, which is series combination of R and L. Load-2 and Load-3 are linear loads with their respective resistances and inductances as shown in Table 4.1.

SunPower SPR-305E-WHT-D, PV module is selected in this work for simulating PV array. Ten such PV modules are connected in series to form a string and five such strings are connected in parallel to form complete PV array. PV model is based on equivalent circuit of solar PV consisting of a controlled current source with diode in parallel, series and shunt resistances, which is best suited for simulation of power electronics circuits with solar PV [18]. Parameters of solar PV array at standard test conditions (1000 W/m^2, 25°) are shown in Table. 4.2.

Table 4.2: Parameters of solar PV array

Maximum Power	15.3 kW
Open circuit voltage	642 V
Short circuit current	30.3 A
Voltage at MPP	547 V
Current at MPP	27.9 A

4.6 Real Time Simulation Results and Discussion

Performance of proposed control of UPQC-DG has been tested for steady state as well as dynamic situations. For evaluating dynamic response, proposed UPQC-DG

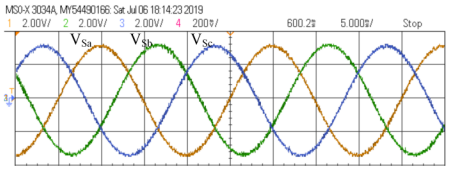

(a) Source voltages, Scale- V_S: 250 V/div., time: 5 ms/div.

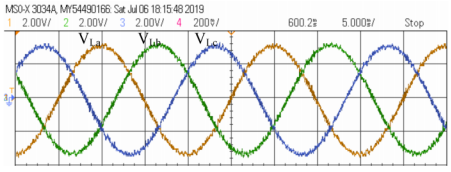

(b) Load voltages, Scale- V_L: 250 V/div., time: 5 ms/div.

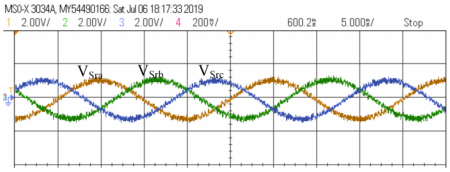

(c) Series APF voltages, Scale- V_{Sr}: 250 V/div., time: 5 ms/div.

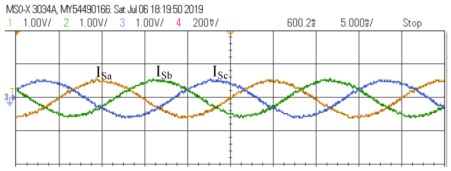

(d) Source currents, Scale- I_S: 50 A/div., time: 5 ms/div.

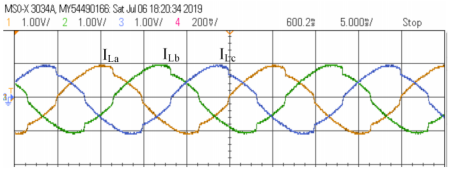

(e) Load currents, Scale- I_L: 50 A/div., time: 5 ms/div.

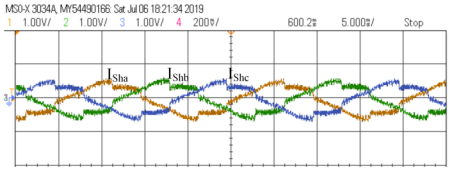

(f) Shunt APF currents, Scale- I_{Sh}: 50 A/div., time: 5 ms/div.

Figure 4.5: Three phase steady state waveforms

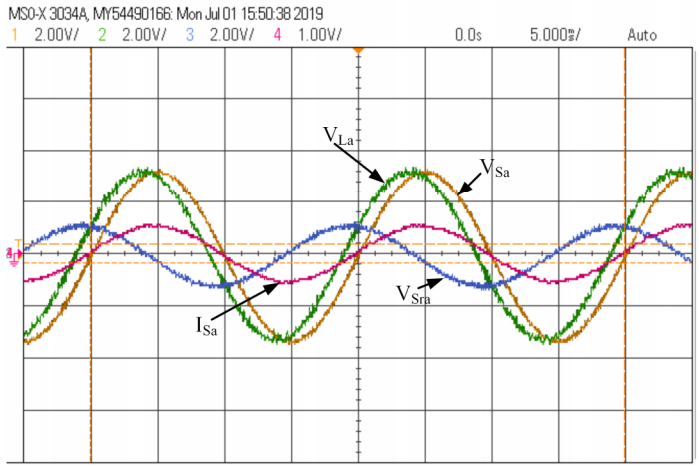

Figure 4.6: Phase differences between phase A of key quantities in steady state

system is simulated for three cases covering variation in solar PV output, variation in supply voltage and change in load. These cases are further described in following sub-sections.

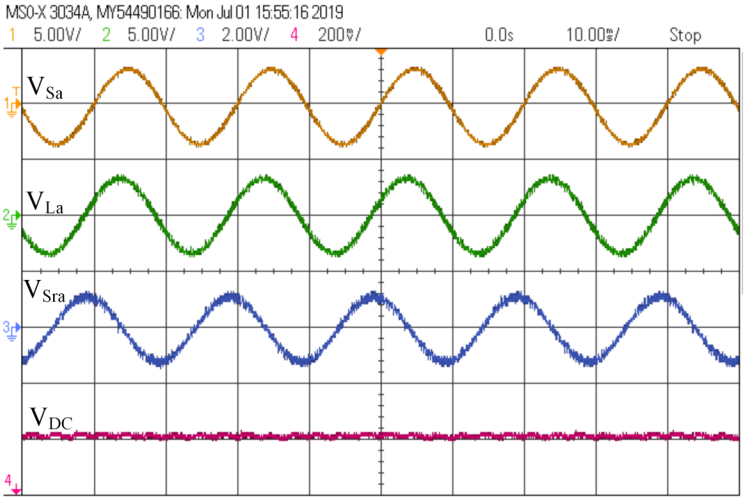

(a) Voltage waveforms in steady state
Scale- V_{Sa}: 500 V/div., V_{La}: 500 V/div., V_{Sra}: 250 V/div., V_{DC}: 25 V/div., time: 5 ms/div.

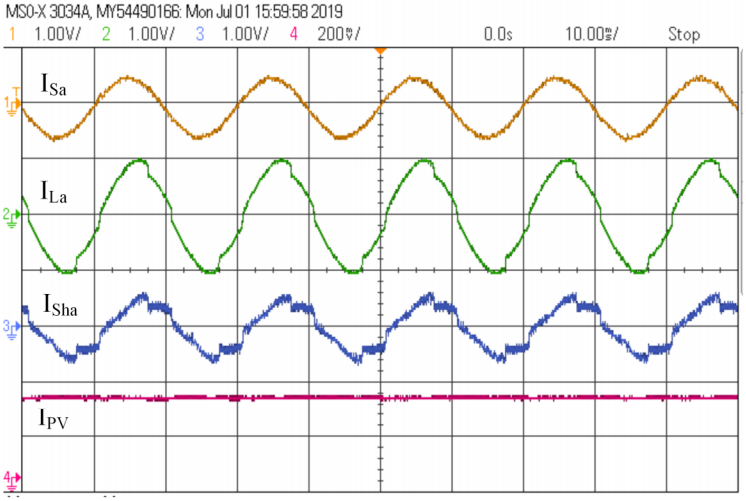

(b) Current waveforms in steady state
Scale- I_{Sa}: 50 A/div., I_{La}: 50 A/div., I_{Sha}: 25 A/div., I_{PV}: 25 A/div., time: 10 ms/div.

Figure 4.7: Steady state waveforms for 0 degree firing angle of controlled rectifier

4.6.1 Steady State Performance

In steady state, all three loads are connected and UPQC-DG is operating under proposed PAC method. Under this PAC method, series APF supplies reactive power demand of load upto its full capacity. Remaining reactive power of load is supplied

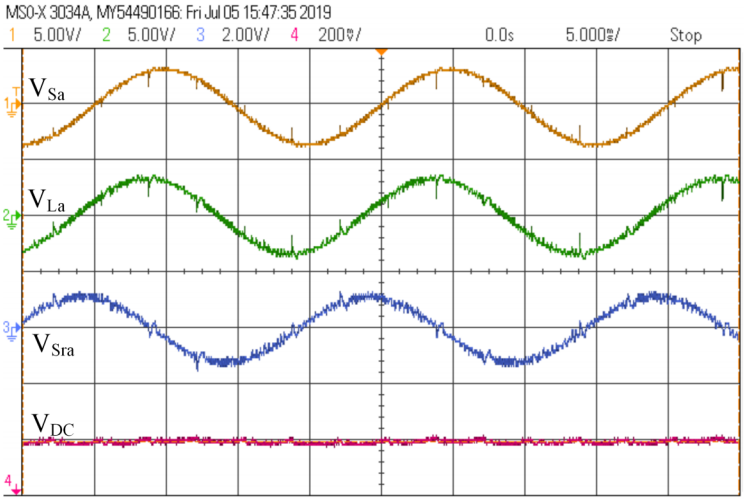

(a) Voltage waveforms in steady state
Scale- V_{Sa}: 500 V/div., V_{La}: 500 V/div., V_{Sra}: 250 V/div., V_{DC}: 25 V/div., time: 5 ms/div.

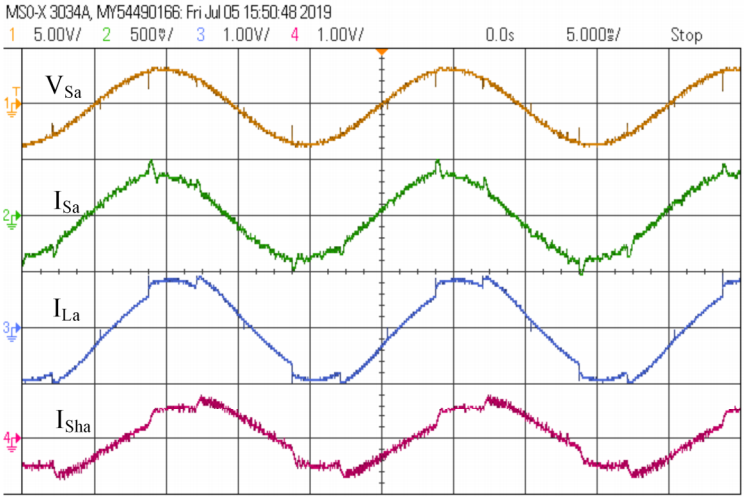

(b) Current waveforms in steady state
Scale- V_{Sa}: 500 V/div., I_{Sa}: 50 A/div., I_{La}: 50 A/div., I_{Sha}: 25 A/div., time: 10 ms/div.

Figure 4.8: Steady state waveforms for 60 degree firing angle of controlled rectifier

by shunt APF, which also compensates for load current harmonics. Three phase steady state waveforms of three phase quantities are shown in Fig. 4.5. Since this is a balanced three phase system, all quantities are balanced.

Phase-A of some key quantities is shown in Fig. 4.6, for visualization of phase differences among these quantities. Due to PAC method of operation there is phase

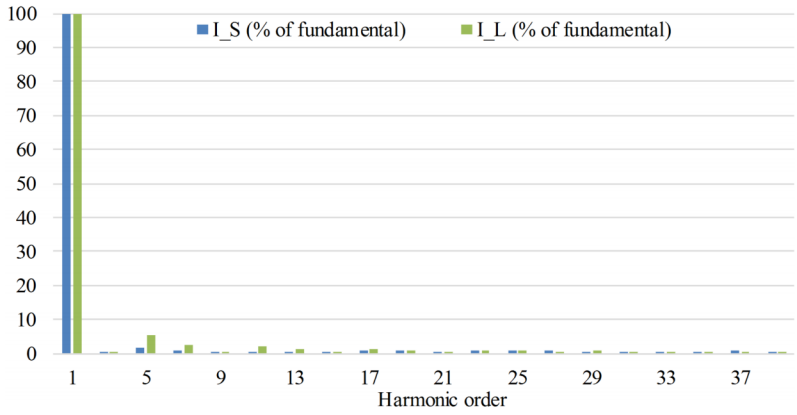

(a) FFT spectrum for 0 degree firing angle

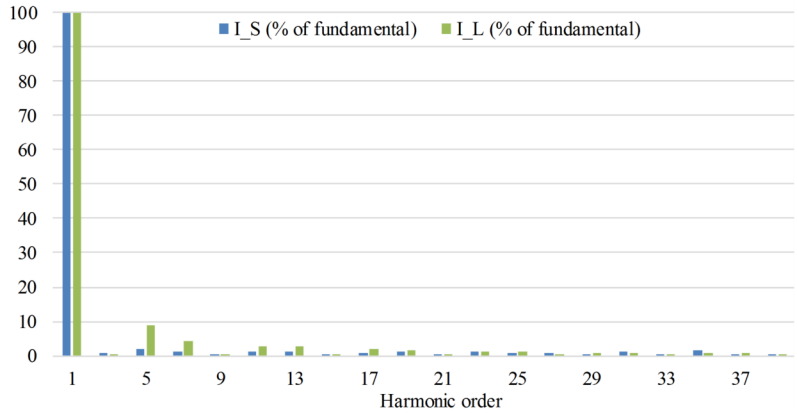

(b) FFT spectrum for 60 degree firing angle

Figure 4.9: FFT spectrum of load and source currents for different cases

difference (power angle) between source voltage (V_{Sa}) and load voltage (V_{La}). Source voltage and source current (I_{Sa}) are in phase confirming unity power factor at source. Voltage injected by series APF (V_{Sra}) is at suitable phase angle with source current to yield desirable power angle of 23.1°, which is maximum achievable with given series APF rating. It also can be observed that series voltage (V_{Sra}) is almost in quadrature with source current, indicating that series APF mainly injects reactive power with negligible active power exchange to meet power losses.

DC link voltage is maintained constant at its reference value by PI controller of shunt APF during steady state operation (Fig. 4.7a). Apart from supplying part of load reactive power, shunt APF also compensates for harmonics in load current and maintains sinusoidal source currents (Fig. 4.7b). Total Harmonic Distortion (THD) value of source current is found within 5% as per IEEE-519 standards. PV output

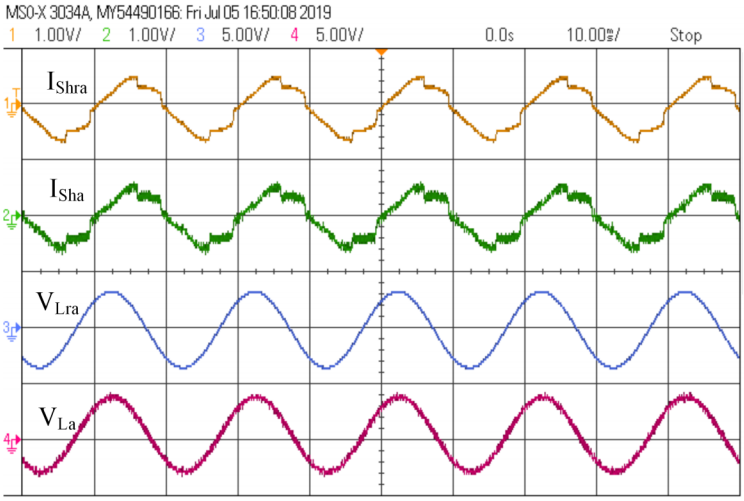

(a) Shunt APF reference current
Scale- I_{Shra}: 50 A/div., I_{Sha}: 50 A/div., I_{La}: 100 A/div., I_{Sa}: 100 A/div., time: 20 ms/div.

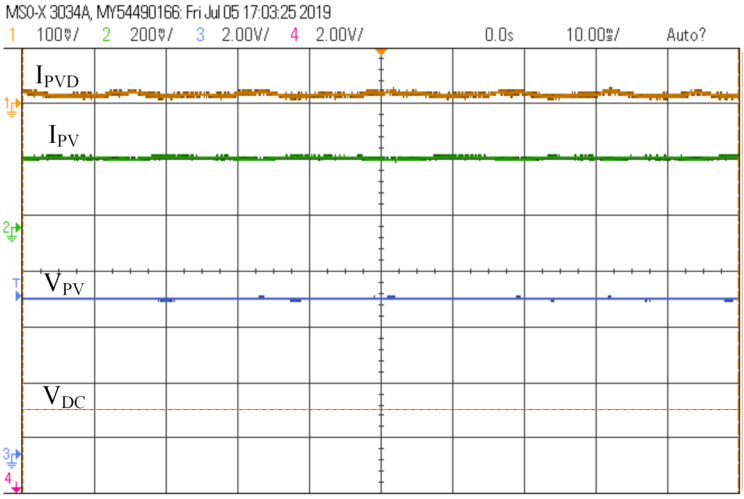

(b) Solar PV and boost converter quantities
Scale- I_{PV}: 25 A/div., V_{PV}: 250 V/div., V_{DC}: 100 V/div., time: 10 ms/div.

Figure 4.10: Additional steady state waveforms for 0 degree firing angle case

current is DC and remains constant during observation.

Performance of proposed system is also validated for different set of load current harmonics, which results due to change in firing angle of thyristor bridge rectifier. To create such a condition, firing angle of thyristors is changed to 60 degree, and obtained voltage and current waveforms are shown in Fig.4.8. It can be observed

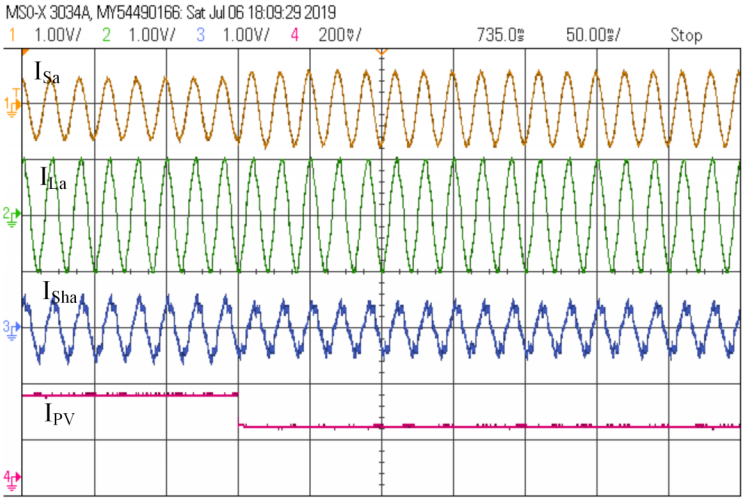

(a) Current waveforms during variation in solar irradiation
Scale- I_{Sa}: 100 A/div., I_{La}: 100 A/div., I_{Sha}: 50 A/div., I_{PV}: 50 A/div., time: 20 ms/div.

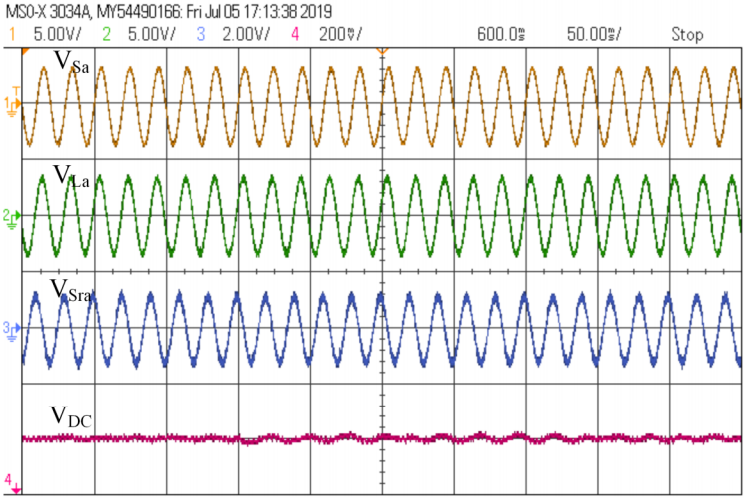

(b) Voltage waveforms in during variation in solar irradiation
Scale- V_{Sa}: 500 V/div., V_{La}: 500 V/div., V_{Sra}: 250 V/div., V_{DC}: 10 V/div., time: 20 ms/div.

Figure 4.11: Transient performance during variation in solar irradiation

that load current has different shape in comparison to Fig.4.7b. In spite of this change source current still remains fairly sinusoidal.

Firing angle of thyristor rectifier is also changed to 30 degree and performance of UPQC-DG is observed. FFT analysis for source and load current has been carried out for all three cases of firing angle of thyristor rectifier and THD results are presented

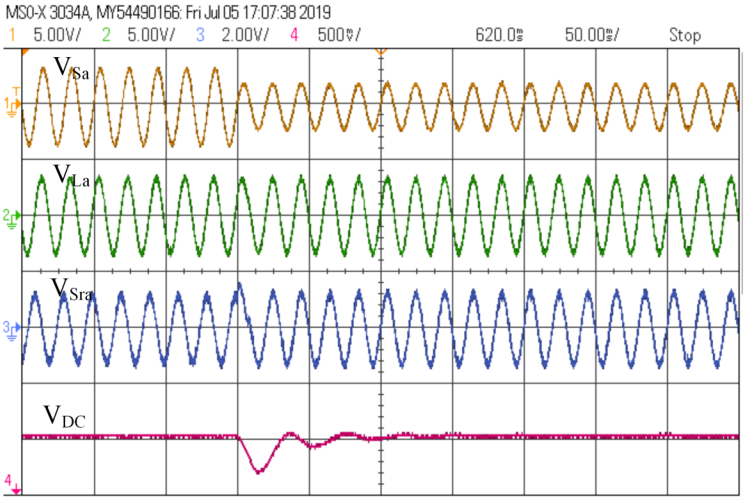

(a) Voltage waveforms during sag
Scale- V_{Sa}: 500V/div, V_{La}: 500V/div, V_{Sra}: 250V/div, I_{Sa}: 75 A/div., time: 5 ms/div.

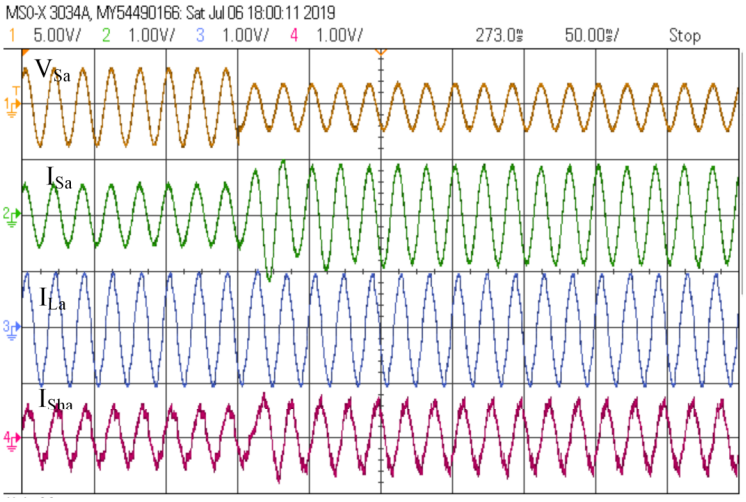

(b) Current waveforms during sag
Scale- V_{Sa}: 500 V/div., I_{Sa}: 50 A/div., I_{La}: 50 A/div., I_{Sha}: 50 A/div., time: 10 ms/div.

Figure 4.12: Transient waveforms during sag in supply voltage

in Table 4.3. Source current THD is found to be well within 5% in each case. It can be observed from the table that though 30 & 60 degree cases have lower load current THDs than in case of 0 degree, source currents THDs are higher in case 30 & 60 degrees. This is because of increased lower order harmonic contents in load current in those cases. These lower order notches can be seen in voltage and current

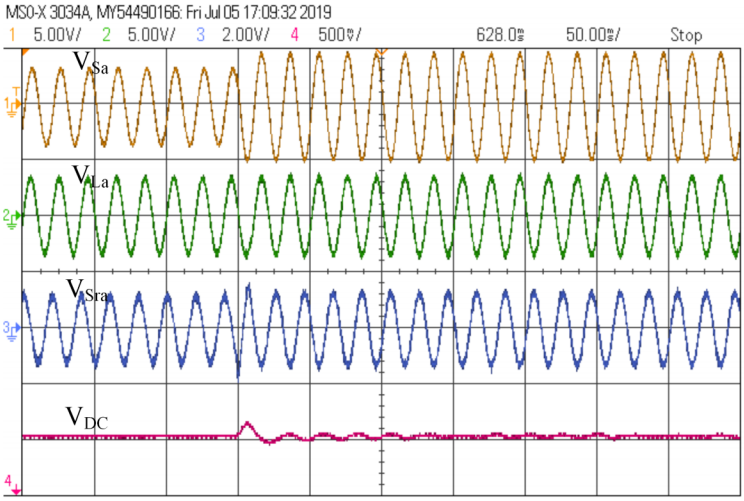

(a) Voltage waveforms during swell
Scale- V_{Sa}: 500V/div, V_{La}: 500V/div, V_{Sra}: 250V/div, I_{Sa}: 75 A/div., time: 5 ms/div.

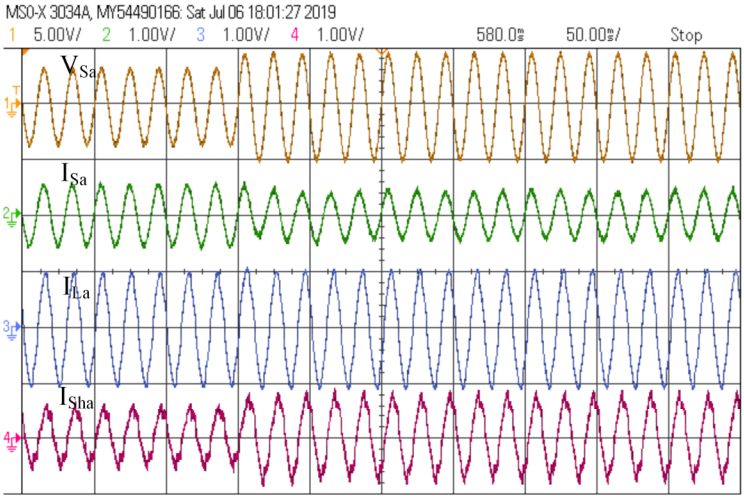

(b) Current waveforms during swell
Scale- V_{Sa}: 500 V/div., I_{Sa}: 50 A/div., I_{La}: 50 A/div., I_{Sha}: 50 A/div., time: 10 ms/div.

Figure 4.13: Transient waveforms during swell in supply voltage

waveforms in Fig. 4.8. FFT spectrum of currents for firing angle of 0 and 60 degree is shown in Fig. 4.9.

Additional waveforms for steady state are shown in Fig. 4.10. Reference current of shunt APF (I_{Shra}), along with other currents in system is plotted in single screen-shot in Fig. 4.10a. Actual current of shunt APF (I_{Sha}) follows reference current, but

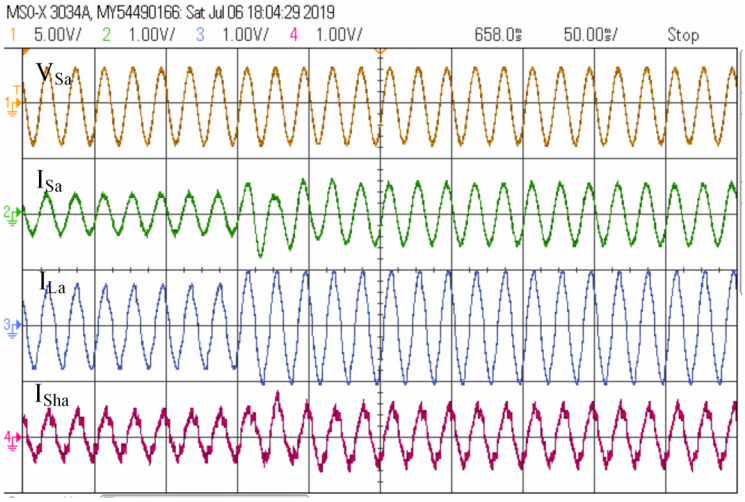

(a) Current waveforms during change in load
Scale- V_{Sa}: 500V/div, V_{La}: 500V/div, V_{Sra}: 250V/div, I_{Sa}: 75 A/div., time: 5 ms/div.

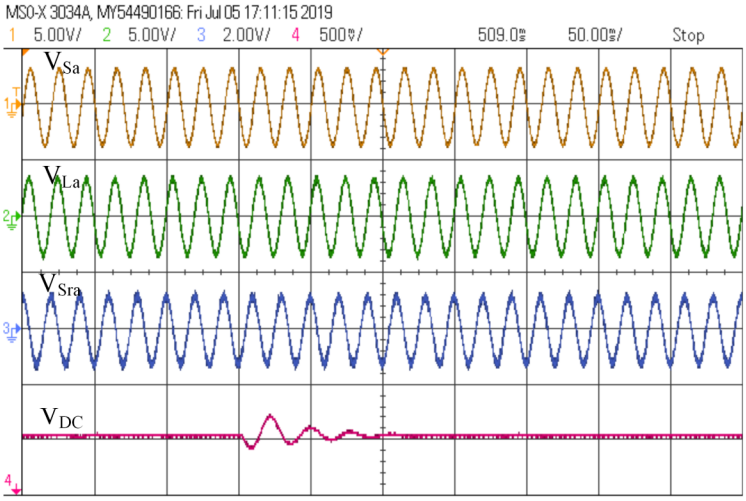

(b) Voltage waveforms during change in load
Scale- V_{Sa}: 500 V/div., I_{Sa}: 50 A/div., I_{La}: 50 A/div., I_{Sha}: 50 A/div., time: 10 ms/div.

Figure 4.14: Transient Performance during change in load

contains high frequency components due to switching. Output voltage of PV array, along with PV current and DC link voltage is shown in Fig. 4.10b. It is to be noticed that PV current is also the inductor current of DC-DC converter, which is operating in continuous conduction mode. Also, PV output voltage and DC link voltage are input and output voltage of boost converter respectively.

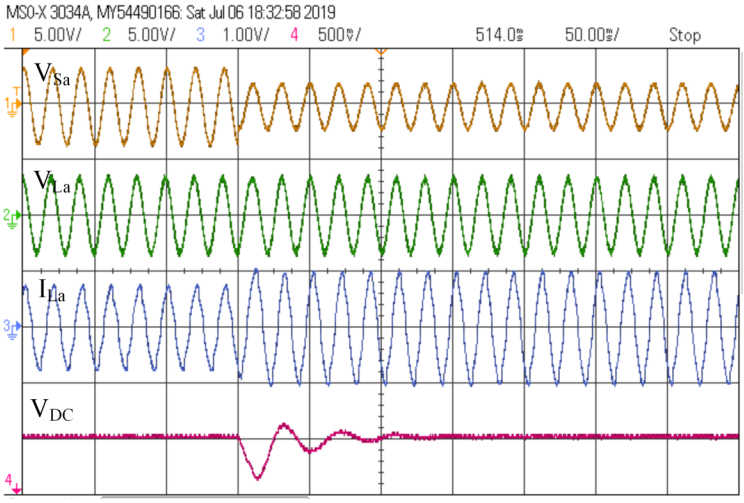

(a) Current waveforms
Scale- V_{Sa}: 500 V/div., V_{La}: 500 V/div., I_{La}: 100 A/div., V_{DC}: 25 V/div., time: 5 ms/div.

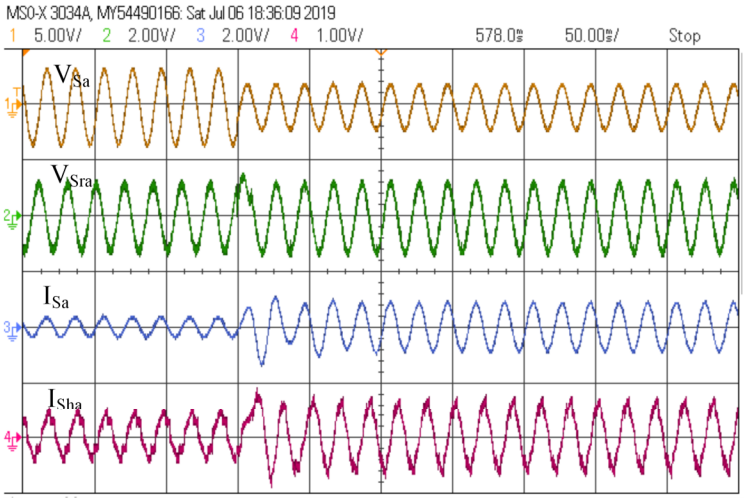

(b) Voltage waveforms
Scale- V_{Sa}: 500 V/div., V_{Sra}: 250 V/div., I_{Sa}: 100 A/div., I_{Sha}: 50 A/div., time: 10 ms/div.

Figure 4.15: Transient Performance during simultaneous voltage sag and increase in load

4.6.2 Performance during Variation in Solar Irradiation

For testing performance of proposed UPQC-DG during variation in solar irradiation, irradiation is varied in step fashion from 1000 W/m^2 to 600 W/m^2 (Fig. 4.11), keeping other system conditions same as those in steady state. Due to the reduction in

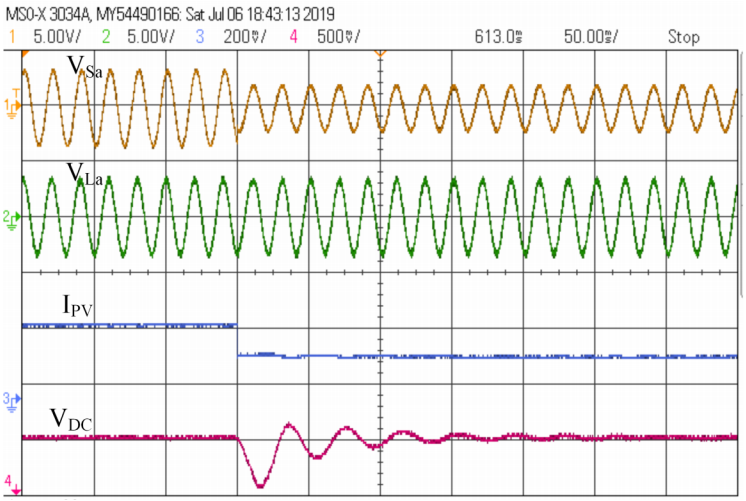

(a) Current waveforms
Scale- V_{Sa}: 500 V/div., V_{La}: 500 V/div., I_{PV}: 25 A/div., V_{DC}: 25 V/div., time: 5 ms/div.

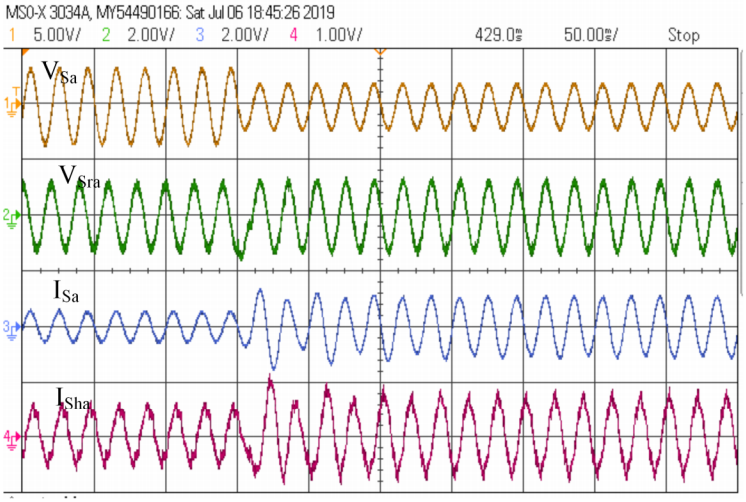

(b) Voltage waveforms
Scale- V_{Sa}: 500 V/div., V_{Sra}: 250 V/div., I_{Sa}: 100 A/div., I_{Sha}: 50 A/div., time: 10 ms/div.

Figure 4.16: Transient Performance during simultaneous voltage sag and decrease in solar irradiation

irradiation, current injected by solar PV reduces proportionately. Reduction in PV current leads to reduction in fundamental in-phase component of shunt APF current (I_{Sha}), but reactive and harmonic components remain unaltered. As a result, source current power quality is maintained, and THD of source current is found to be 2.84%.

Table 4.3: THD value of load and source current for different cases

Case	Load current THD (%)	Source current THD (%)
Firing angle = 0 degree (full load)	7.07	3.17
Firing angle = 30 degree (partial load)	9.67	3.52
Firing angle = 60 degree (partial load)	11.03	4.28

Since load power is fixed source current increases smoothly as PV power output reduces. Load current doesn't experience the variations in solar PV power output. Except slight change, DC link voltage is held at constant value (700 V) during variation in solar irradiation.

4.6.3 Performance during Sag in Supply Voltage

To simulate sag in supply voltage, a sag of 25% magnitude is considered (Fig. 4.12). During the sag in supply voltage, load voltage magnitude is maintained constant, by injecting suitable voltage through series APF. During sag, phase angle and magnitude of series voltage changes because now it has to supply a voltage component in phase with source voltage to compensate for sag. Due to this in phase component series APF injects active power due to which DC link voltage starts falling but this reduction is compensated by PI controller. Also, PV power is utilized in maintaining the DC voltage from falling down. So, current (thus active power) injected by shunt APF reduces, and source current increases to maitain load current.

4.6.4 Performance during Swell in Supply Voltage

To simulate sag in supply voltage, a swell of 25% magnitude is considered (Fig. 4.13). During the swell in supply voltage, load voltage magnitude is maintained constant, by injecting suitable voltage through series APF. During swell, phase angle and magnitude of series voltage changes because now it has to supply a voltage component out of phase with source voltage to compensate for sag. Due to out of phase injection of series voltage, series APF consumes active power due to which, DC link voltage has tendency to increase, but this increase is compensated by PI controller. Active power consumed by series APF is fed back to load via shunt APF. Thus shunt APF injects more current including current from PV, making source current to reduce.

4.6.5 Performance during Change in Load

A step change in load is simulated by disconnection of load-3. Real time simulation results are shown in Fig.4.14. Due to step change in load, total reactive power demand reduces to only 4.45 kVAr, which is supplied by series APF alone as it lies within the capacity of series APF. Magnitude of series voltage reduces due to decrease in reactive power supplied by series APF. DC link voltage is held fixed except for slight variations. Current injected by shunt APF remains constant except for some distortions due to DC link voltage variation. Current drawn from source also reduces upon disconnection of load-3.

4.6.6 Performance during Simultaneous Disturbances

Simultaneous disturbances can easily occur in renewable DG based systems, such as proposed UPQC-DG. Out of many possible simultaneous disturbances, most probable ones are considered in this work. First simultaneous disturbance is voltage sag and increase in load. Waveforms for this case are shown in Fig. 4.15. During sag load voltage is maintained fairly constant. DC link voltage experiences undershoot and overshoot, but settles soon. Series APF voltage increases to cater to increased reactive power demand as well as to compensate sag. Due to sag and increase in load, source current increases. Fundamental component of shunt APF current reduces, since part of PV power is fed through series APF during sag.

Another simultaneous disturbance considered in this work, is sag and reduction in solar irradiation (Fig. 4.16). Load voltage is maintained constant during sag. Except small oscillations, DC link voltage is maintained at set value of 700 V. Series APF voltage changes to compensate for sag, in addition to supply reactive power. Due to reduction in PV power and sag in supply voltage, fundamental component of shunt APF current reduces, and source current increases.

4.6.7 Analysis of power sharing during different operating conditions

Real time simulation is also performed for UPQC-DG without PAC control, and a comparison of VA loadings of series and shunt APFs with and without PAC control is presented in Table. 4.4. This comparison has been made while keeping thyristor bridge firing angle to zero. It can be observed from the table that during steady state,

shunt APF is heavily loaded and series APF is under utilized without PAC approach. With PAC approach, series APF of UPQC-DG supplies part of load reactive power determined by proposed control algorithm. So, with proposed PAC control, VA capacity utilization for series APF is 35.0% and that for shunt APF is 62.2%, under steady state operation. Whereas without PAC, VA capacity utilization for series APF is only 1.8% and that for shunt APF is 81.7%. In effect VA capacity of series APF is properly utilized and shunt APF loading is reduced by 23.8% using proposed PAC.

Following the reduction in solar irradiation, it can be observed that proposed PAC control still offers better VA sharing between two APFs. VA loadings of series and shunt APFs, following the change in load, given in Table. 4.4, show that proposed PAC has better sharing of VA load between two APFs.

Table 4.4: Comparison of VA loadings of series and shunt APFs of UPQC-DG with and without PAC control for different operating conditions

Test-Case and Method	S_L (kVA)	S_{Sr} (kVA)	$\|S_{Sr}\|$ (kVA)	S_{Sh} (kVA)	$\|S_{Sh}\|$ (kVA)
Steady state with PAC	41.5 + j29.6	-1.4 + j9.7	9.8	15.1 + j20.9	25.8
Steady state without PAC	41.5 + j29.6	0.0 − j0.5	0.5	13.8 + j31.0	33.9
Reduced irradiation with PAC	41.5 + j29.6	-1.8 + j11.6	11.7	9.2 + j18.8	20.9
Reduced irradiation without PAC	41.5 + j29.6	0.0 − j0.8	0.8	7.5 + j31.2	32.1
Voltage sag with PAC	40.3 + j28.8	17.2 − j1.8	17.3	-4.0 + j30.2	30.5
Voltage sag without PAC	40.3 + j28.8	17.2 − j1.8	17.3	-4.0 + j30.2	30.5
Voltage swell with PAC	44.3 + j31.8	-8.3 + j0.5	8.3	22.1 + j32.1	38.9
Voltage swell without PAC	44.3 + j31.8	-8.3 + j0.3	8.3	22.1 + j32.4	39.2
Load-3 off with PAC	31.9 + j20.0	-0.6 + j6.6	6.6	14.4 + j14.4	20.4
Load-3 off without PAC	31.9 + j20.0	0.0 − j0.2	0.2	13.8 + j20.7	24.9

4.7 Summary

In this chapter, a new SRF based PAC method for control of UPQC-DG is proposed for grid integration of solar PV. Proposed PAC method shares reactive power burden of load between series and shunt APF and gives better utilization of kVA ratings of series and shunt APFs in comparison to control of UPQC-DG without PAC approach. Simulation results show 23.8% reduction in kVA loading of shunt APF in steady state by using proposed PAC approach. Dynamic performance of proposed PAC method has been tested during variation in solar irradiation, supply voltage disturbances and change in load, and is found to have superior power sharing between two APFs of

UPQC-DG than conventional control without PAC. Performance of proposed control is also validated in presence of simultaneous disturbances. In spite of various power quality disturbances, quality power is supplied to load and supply currents are maintained undistorted with unity power factor. Multi-step real time simulation performed in Opal-RT has validated effectiveness of proposed method.

Bibliography

[1] V. Khadkikar, "Enhancing electric power quality using UPQC: A comprehensive overview," *IEEE Transactions on Power Electronics*, vol. 27, no. 5, pp. 2284–2297, 2012.

[2] T. Koroglu, K. C. Bayindir, and M. Tumay, "Performance analysis of multiconverter unified power quality conditioner with an EPLL-based controller at medium voltage level," *International Transactions on Electrical Energy Systems*, vol. 26, no. 12, pp. 2774–2786, 2016.

[3] A. R. Reisi, M. H. Moradi, and H. Showkati, "Combined photovoltaic and unified power quality controller to improve power quality," *Solar Energy*, vol. 88, pp. 154–162, 2013.

[4] V. Madhaiyan and V. Subramaniam, "Extended reference signal generation scheme for integration of unified power quality conditioner in grid-connected photovoltaic system," *Electric Power Components and Systems*, vol. 43, no. 8-10, pp. 914–927, 2015.

[5] A. Shrivastava and P. Nene, "Power quality enhancement using UPQC connected with PV arrays," in *Proc. 5th IEEE Communication Systems and Network Technologies*, 2015, pp. 1232–1237.

[6] S. Devassy and B. Singh, "Dynamic performance of solar PV integrated UPQC-P for critical loads," in *Proc. 12th IEEE India Council International Conference*, 2015, pp. 1–6.

[7] A. Patel and P. Chaturvedi, "Performance of SRF-UVTG based UPQCDG for integration of solar PV with non-linear loads," in *Proc. 7th IEEE Power Electronics, Drives and Energy Systems Conference*, 2016, pp. 1–5.

[8] V. Khadkikar and A. Chandra, "A new control philosophy for a unified power quality conditioner (UPQC) to coordinate load-reactive power demand between shunt and series inverters," *IEEE Transactions on Power Delivery*, vol. 23, no. 4, pp. 2522–2534, 2008.

[9] A. K. Panda and N. Patnaik, "Combined operation of a new power angle control unit vector template based unified power quality conditioner and fuel cell stack supply with effective utilization of shunt and series inverter," *Electric Power Components and Systems*, vol. 44, no. 18, pp. 2048–2058, 2016.

[10] V. Khadkikar and A. Chandra, "UPQC- S: A novel concept of simultaneous voltage sag/swell and load reactive power compensations utilizing series inverter of UPQC," *IEEE Transactions on Power Electronics*, vol. 26, no. 9, pp. 2414–2425, 2011.

[11] V. Khadkikar, "Fixed and variable power angle control methods for unified power quality conditioner: operation, control and impact assessment on shunt and series inverter kVA loadings," *IET Power Electronics*, vol. 6, no. 7, pp. 1299–1307, 2013.

[12] N. Patnaik and A. K. Panda, "Performance analysis of a 3 phase 4 wire UPQC system based on PAC based SRF controller with real time digital simulation," *International Journal of Electrical Power & Energy Systems*, vol. 74, pp. 212–221, 2016.

[13] A. K. Panda and N. Patnaik, "Management of reactive power sharing and power quality improvement with SRF-PAC based UPQC under unbalanced source voltage condition," *International Journal of Electrical Power & Energy Systems*, vol. 84, pp. 182–194, 2017.

[14] K. Palanisamy, D. Kothari, M. K. Mishra, S. Meikandashivam, and I. J. Raglend, "Effective utilization of unified power quality conditioner for interconnecting PV modules with grid using power angle control method," *International Journal of Electrical Power & Energy Systems*, vol. 48, pp. 131–138, 2013.

[15] V. Khadkikar, P. Agarwal, A. Chandra, A. Barry, and T. Nguyen, "A simple new control technique for unified power quality conditioner (UPQC)," in *Proc. 11th IEEE International Conference on Harmonics and Quality of Power*, 2004, pp. 289–293.

[16] M. Abdulkadir, A. Samosir, and A. Yatim, "Modelling and simulation of maximum power point tracking of photovoltaic system in Simulink model," in *Proc. IEEE International Conference on Power and Energy*, 2012, pp. 325–330.

[17] T. Ould-Bachir, H. F. Blanchette, and K. Al-Haddad, "A network tearing technique for FPGA-based real-time simulation of power converters," *IEEE Transactions on Industrial Electronics*, vol. 62, no. 6, pp. 3409–3418, 2015.

[18] M. G. Villalva, J. R. Gazoli, and E. Ruppert Filho, "Comprehensive approach to modeling and simulation of photovoltaic arrays," *IEEE Transactions on Power Electronics*, vol. 24, no. 5, pp. 1198–1208, 2009.